energies

MDPI

Article

Tabulated Chemistry Combustion Model for Cost-Effective Numerical Simulation of Dual-Fuel Combustion Process

Marija Stipic [1,*], Branislav Basara [1], Steffen J. Schmidt [2] and Nikolaus A. Adams [2]

[1] AVL List GmbH, 8020 Graz, Austria; branislav.basara@avl.com
[2] Chair of Aerodynamics and Fluid Mechanics, Technical University of Munich, D-85748 Garching, Germany; steffen.schmidt@tum.de (S.J.S.); nikolaus.adams@tum.de (N.A.A.)
* Correspondence: marijas176@gmail.com

Abstract: This study is dedicated to improving the efficiency of the flamelet-generated manifold (FGM) tabulated chemistry combustion modeling approach for predicting the combustion process in diesel-ignited internal combustion (IC) engines. The primary focus is on reducing table generation time and memory requirements. To accurately predict dual-fuel combustion processes, it is important to model both premixed and non-premixed combustion regimes. However, attempting to include both regimes in a single FGM lookup table leads to significant increases in the table size and generation time. In response, this work proposes a dual-table configuration, with each table dedicated to a specific regime. The solution is then interpolated from these tables based on the calculated combustion regime indicator during the computational fluid dynamics (CFD) simulation. This approach optimizes computational efficiency while ensuring an accurate representation of dual-fuel combustion. Additionally, to establish a cost-effective and accurate 3D CFD simulation workflow, the dual-table FGM methodology is coupled with the partially averaged Navier–Stokes (PANS) turbulence model. The feasibility of the proposed FGM methodology is tested utilizing six chemical kinetics mechanisms with different levels of detail. The results of this study demonstrated that the dual-table approach significantly accelerates table generation time and reduces memory requirements compared to a single table that includes both combustion regimes. Furthermore, 3D CFD simulation results of the dual-fuel combustion process are validated against available experimental data for three engine operating points. The in-cylinder pressure traces and rate of heat release obtained from the 3D CFD simulations employing the FGM PANS methodology show good agreement with experimental measurements, confirming the accuracy and reliability of this modeling approach.

Keywords: dual fuel; 3D CFD simulation; flamelet-generated manifold; partially averaged Navier–Stokes turbulence model

Citation: Stipic, M.; Basara, B.; Schmidt, S.J.; Adams, N.A. Tabulated Chemistry Combustion Model for Cost-Effective Numerical Simulation of Dual-Fuel Combustion Process. *Energies* **2023**, *16*, 8040. https://doi.org/10.3390/en16248040

Academic Editors: Gholamreza Kefayati and Hasan Sajjadi

Received: 5 November 2023
Revised: 23 November 2023
Accepted: 30 November 2023
Published: 13 December 2023

1. Introduction

According to [1], today's world population is more than three times larger than it was in the mid-twentieth century, and it is still growing. The continuous growth of population, together with the expansion of urbanization, rapid industrialization and economic development, is associated with constantly increasing energy consumption, consumer demands, and an increased need for industrial goods. These factors necessitate an increase in the future demand for services provided by the road freight sector. Indeed, it has been reported in [2] that while the oil consumption and energy use of the road passenger vehicle fleet have begun to plateau and decline, oil use by the road freight sector has continued to increase. Although the electrification of vehicles is mandated by economic, social and geopolitical trends, no electrification strategy for heavy-duty vehicles is foreseen. One of the favored polices to reduce significant harmful climate and air quality impacts from road freight transport is the utilization of the dual-fuel internal combustion (IC) engine. Indeed, as stated in [3], dual-fuel IC engines can be utilized in applications where electrification is not deemed to be a viable solution to tackle emission issues. These applications include

cargo ships, heavy-duty trucks and marine engines. The concept of dual-fuel combustion has attracted growing interest, primarily due to its fuel flexibility and its ability to achieve lower NO_x and soot emissions compared to conventional diesel engines [4]. The focus of this paper is the diesel ignited gas engine. This type of engine is operated by burning a premixed natural gas/air mixture ignited with a small amount of directly injected diesel fuel. This concept has several disadvantages, which are discussed in [5]. Nevertheless, dual-fuel engines are the subject of active research, and establishing an effective design process for dual-fuel engines and its fuel injection equipment represents a key priority.

By leveraging advanced simulation technologies, the cost and time required for the development of dual-fuel IC engine and its fuel injection equipment can be significantly reduced. In particular, 3D computational fluid dynamics (CFD) simulation tools have long been utilized for the design of IC engines due to their potential to offer accurate predictions of the combustion process with a reduced number of prototypes in the development and test phases. Nevertheless, the combustion process involves strong coupling between chemistry, transport and fluid dynamics [6]. Hence, simulating turbulent combustion is, to date, a challenging task. In addition, the dual-fuel engine combines the characteristics of both the compression and spark ignition engine operational modes. Hence, all combustion regimes (i.e., autoignition, diffusion combustion and premixed flame front propagation) have to be modelled simultaneously [7]. Furthermore, the introduction of gaseous fuel in the combustion chamber strongly modifies mixture formation and the combustion properties of the pilot diesel spray, which is utilized as an ignition agent [8]. The work of several authors, both experimental [9,10] and numerical [4,7] has shown that the ignition delay time of pilot diesel fuel strongly depends on the fuel mixture fraction of natural gas and diesel. These challenges strongly rely on the chemical kinetics of the gaseous fuel–air mixture, which, in turn, varies based on the type and concentration of used gaseous fuel, as well as the quantity of the employed pilot fuel. Thus, numerical modeling of dual-fuel combustion is a complex task. The process can be accurately depicted by utilizing detailed chemical reaction schemes that involve necessary reactions to the estimated consumption rates of both fuels. A detailed understanding of chemistry is essential for the correct prediction of the ignition, stabilization or extinction of reaction zones, as well as for understanding the formation of harmful pollutants. Since detailed chemical mechanisms can involve thousands of chemical species and elementary reactions, a direct resolution of the combustion process's chemistry requires significant computational power. For the numerical simulation of industrial interest, this computational cost is not affordable. This has led to the development of reduced chemical kinetic mechanisms and combustion models capable of providing faster results. In the work of several authors [11,12], reduced chemical kinetic mechanisms for CFD simulation of natural gas/diesel dual-fuel engines have been developed. However, even with the reduced chemistry, simulation of the combustion process in IC engines of industrial interest is limited to the Reynolds-averaged Navier–Stokes (RANS) turbulence modeling framework due to the long computational time [4]. On the other hand, combustion models can provide valuable results under significantly lower computational effort compared to the detailed chemistry simulation. A successful framework for the simulation of the dual-fuel combustion process based upon the three-zone extended coherent flame model is presented in [4,13]. Nevertheless, simplified combustion models sacrifice some level of accuracy to achieve computational efficiency. Indeed, to gain a deeper understanding of the dual-fuel combustion process, including pollutant emissions and flame characteristics, under various operating conditions, detailed chemical kinetics should be employed. With the aim of combining detailed chemical kinetics with computational efficiency, in this study, the tabulated chemistry combustion modeling approach has been employed to predict the combustion process in a large, single-cylinder, dual-fuel IC engine. More specifically, the focus of this paper is the flamelet-generated manifold (FGM) tabulated chemistry approach. The FGM combustion model makes use of the lookup tables generated using the chemical kinetics mechanism with any degree of detail. The pre-tabulation approach ensures affordable computational times without loss of accuracy due to combustion modeling. Thus, the

FGM model is ideally suited for 3D CFD simulation of IC engines. The model has proven its capability to predict the combustion process in both diesel [14,15] and gasoline [16] IC engines. To adequately capture turbulence chemistry interactions (TCI), the model relies on a priori assumptions regarding the occurring combustion regime, either premixed or non-premixed. As already stated, dual-fuel combustion involves the combination of combustion regimes. However, simultaneous consideration of the premixed and non-premixed combustion regimes in the same lookup table would significantly increase computational efforts with respect to the memory and table generation time demands. Therefore, the work presented here makes use of two lookup tables (one for the premixed and one for the non-premixed regime) and interpolates the solution from the tables based on the value of the combustion regime indicator calculated during CFD simulation. The methodology for handling multiple fuels within the FGM tabulated chemistry approach is described in detail in Section 2.2.

In addition, resolving the entire range of spatial and temporal scales that characterize turbulent flames in realistic geometries is not computationally tractable even with state-of-the-art computing resources. Consequently, a common practice for turbulent simulation of industrial interest is to adopt the RANS turbulence modeling approach. However, RANS models are single-point closures, relying on the assumption of self-similarity of the turbulence spectrum [17]. This assumption suggests that the complete turbulence spectrum can be defined by a single characteristic turbulent length scale. Hence, the physics of the flow dominated by the organized, large-scale coherent structures cannot be captured satisfactorily [18]. On the other hand, large eddy simulation (LES) can offer a significant advantage over RANS modeling approaches, such as studying cycle-to-cycle variations, which provide more design sensitivity for investigating geometrical and operational changes and produce more detailed results [19]. Nevertheless, the penalty for the increased range of resolved flow structures is the substantial increase in computational demand. Therefore, the work presented here aims to employ a hybrid RANS/LES modeling approach to combine the benefits of a computationally affordable RANS approach and high-fidelity and detailed LES approach for practical engineering applications. An emerging hybrid turbulence modeling approach that has demonstrated its potential in recent years is the partially averaged Navier–Stokes (PANS) method. PANS is designed to capture essential, large-scale fluctuations while modeling the remaining flow scales. As a result, it offers enhanced outcomes compared to the RANS method, while demanding significantly less computational resources than LES calculations. The successful implementation of the PANS technique has been demonstrated across a wide range of applications (see [17,20–22]). Various PANS variants have been developed to date; for this study, a PANS model based on the $k-\zeta-f$ model proposed by Basara et al. [23] is coupled with the FGM tabulated chemistry combustion model.

The aim of this study is to propose a cost-effective 3D CFD simulation workflow for predicting a dual-fuel combustion process suitable for everyday industrial use. The proposed simulation workflow enables the consideration of detailed chemistry effects during dual-fuel combustion and provides more insight into the turbulent combustion process due to resolving the portion of flow fluctuations. Potential benefits of the proposed FGM methodology for dual-fuel combustion based on two lookup tables have been tested on a wide range of chemical mechanisms with different levels of detail. Additionally, the FGM PANS 3D CFD simulation workflow for numerical simulation of dual-fuel combustion has been validated against available experimental data from a single-cylinder, large diesel ignited gas engine.

2. Mathematical Model

The subsequent subsections will provide a comprehensive overview of the numerical models relevant to this study. Firstly, description of the PANS $k-\zeta-f$ model is given. Secondly, the concept of tabulated chemistry modeling approach and derivation of the methodology for dual-fuel applications is elaborated. Finally, the last subsection provides

an analysis of the feasibility of the dual-table approach in comparison to the single-table approach, focusing on aspects such as table generation time and memory size.

2.1. Partially Averaged Navier–Stokes Turbulence Model

The focus of this work is the partially averaged Navier–Stokes (PANS) turbulence model. The PANS model (see references [24,25]) is a bridging scale resolving method that provides a more affordable solution than LES while being more accurate than RANS [23]. The PANS model is based on a so-called "partial averaging concept", in which only a part of the fluctuating scales is filtered. Hence, the instantaneous velocity (V_i) and pressure fields (p) are decomposed into partially filtered components (U_i and P) and unresolved components (u_i and p') as follows:

$$V_i = U_i + u_i\,; \quad p = P + p'. \tag{1}$$

The three-dimensional, unsteady Navier–Stokes equation for the partially averaged velocity evolves to

$$\frac{\partial U_i}{\partial t} + U_j\frac{\partial U_i}{\partial x_j} + \frac{\partial \tau(V_i, V_j)}{\partial x_j} = -\frac{1}{\rho}\frac{\partial P}{\partial x_i} + \nu\frac{\partial^2 U_i}{\partial x_j \partial x_j}. \tag{2}$$

To close the system of partially averaged Navier Stokes equations, a closure for sub-scale stress $\tau(V_i, V_j)$ is needed. The closure model has to consider the influence of unresolved motion on the resolved flow field. As proposed by [24], the closure is obtained by utilizing the Boussinesq approximation as follows:

$$\tau(V_i, V_j) = -\nu_u\left(\frac{\partial U_i}{\partial x_j} + \frac{\partial U_j}{\partial x_i}\right) + \frac{2}{3}k_u\delta_{ij}, \tag{3}$$

where the eddy viscosity of unresolved scales is defined as

$$\nu_u = C_\mu\frac{k_u^2}{\varepsilon_u}. \tag{4}$$

Two additional equations have to be solved to formulate the PANS eddy viscosity, namely the unresolved turbulent kinetic energy k_u and its dissipation rate ε_u. The PANS variant employed in this work is based on the four equations $k-\zeta-f$ RANS turbulence model, which solves an additional equation for the velocity scale ratio (see reference [26]). The RANS $k-\zeta-f$ model is chosen as a starting point for the development of the PANS model due to its high-fidelity near-wall behavior in complex flows. The model development and its advantages are described in detail in [27]; here, equations for the unresolved turbulent kinetic energy, unresolved eddy dissipation and wall-normal unresolved velocity scale ratio are shown in their final form:

$$\frac{\partial k_u}{\partial t} + U_j\frac{\partial k_u}{\partial x_j} = (P_u - \varepsilon_u) + \frac{\partial}{\partial x_j}\left[\left(\nu + \frac{\nu_r}{\sigma_k}\right)\frac{\partial k_u}{\partial x_j}\right], \tag{5}$$

$$\frac{\partial \varepsilon_u}{\partial t} + U_j\frac{\partial \varepsilon_u}{\partial x_j} = C_{\varepsilon 1}P_u\frac{\varepsilon_u}{k_u} - C_{\varepsilon 2}^*\frac{\varepsilon_u^2}{k_u} + \frac{\partial}{\partial x_j}\left[\left(\nu + \frac{\nu_r}{\sigma_\varepsilon}\right)\frac{\partial \varepsilon_u}{\partial x_j}\right], \tag{6}$$

$$\frac{\partial \zeta_u}{\partial t} + U_j\frac{\partial \zeta_u}{\partial x_j} = f_u - \frac{\zeta_u}{k_u}P_u + \frac{\zeta_u}{k_u}\varepsilon_u(1-f_k) + \frac{\partial}{\partial x_j}\left(\frac{\nu_r}{\sigma_\zeta}\frac{\partial \zeta_u}{\partial x_j}\right), \tag{7}$$

where ν_r is viscosity of the resolved fluctuations and $C_{\varepsilon 2}^* = C_{\varepsilon 1} + \frac{f_k}{f_\varepsilon}(C_{\varepsilon 2} - C_{\varepsilon 1})$. In the formulation of the above equations, two new parameters have been introduced, namely the ratio of unresolved to total turbulent kinetic energy f_k and the ratio of unresolved to

total eddy dissipation f_ε. These parameters define the level of physical resolution. Values of the resolution parameters vary between unity and zero. When the resolution parameters equal unity, the resulting calculation is RANS. As the value of the resolution parameters decreases, more of the fluctuating motion is resolved. In the limit in which f_k and f_ε equal zero, a direct numerical simulation is performed. In this study, $f_\varepsilon = 1$, implying that $\varepsilon_u = \varepsilon$ and that the employed numerical mesh supports the cutoff in the inertial scales range. For a grid-cell size Δ, the f_k parameter is defined according to [23] as follows:

$$f_k \geq \frac{1}{\sqrt{C_\mu}} \left(\frac{\Delta}{\Lambda} \right)^{\frac{2}{3}} > \frac{k_u}{k_{tot}}. \tag{8}$$

This specification enables a dynamic update of the f_k parameter in every cell at the end of every time step depending on the flow conditions and mesh resolution. To calculate the integral length scale Λ required in Equation (8), the total turbulent kinetic energy has to be determined. This can be calculated only after the resolved turbulent kinetic energy is obtained using the following equation:

$$k_r = \frac{1}{2} \left(U_i - \overline{U}_i \right)^2. \tag{9}$$

This is not a practical solution since it involves expensive averaging of the resolved field. Therefore, Basara [23] further improved this model by solving an additional transport equation for resolved turbulent kinetic energy, called the scale supplying variable (SSV), which is written as follows:

$$\frac{\partial k_{ssv}}{\partial t} + U_j \frac{\partial k_{ssv}}{\partial x_j} = (1 - f_k)(P - \varepsilon) + \frac{\partial}{\partial x_j} \left[\left(\nu + \frac{\nu_u}{\sigma_{ku}} \right) \frac{\partial k_{ssv}}{\partial x_j} \right] \tag{10}$$

With a desire to establish an accurate and, for today's industry, affordable 3D CFD simulation workflow to calculate the dual-fuel combustion process, in this work, the PANS $k - \zeta - f$ model is coupled with the FGM combustion model, which has been extended for dual-fuel application.

2.2. Flamelet-Generated Manifold Combustion Model

The computational power required to perform numerical simulation of the combustion process with detailed chemistry often surpasses practical limits, particularly within an industrial environment. This is attributed to complex chemical mechanisms involving thousands of chemical species and reactions. Furthermore, a wide variety of time and length scales present in the simulation of the combustion process, particularly for turbulent flames [28], lead to a stiff system of equations that increase the computational complexity. Despite many challenges, consideration of detailed chemical kinetics is essential to obtain high-fidelity predictions of the combustion process for specific industrial applications, such as IC engines. Flamelet-based chemical reduction techniques show great potential in achieving both efficient and high-fidelity predictions of the combustion process. A model that has proven to be a powerful tool for IC engine simulation over the years, in both regimes, premixed [16] and non-premixed [14,15], is the flamelet-generated manifold (FGM) combustion model. The FGM model is a combination of the flamelet and manifold modeling approaches. A recent review of the model can be found in [29]. The model assumes that a turbulent flame is an ensemble of one-dimensional flamelets. The flamelets are pre-computed considering diffusion and convection effects, and the relevant data are stored in a lookup table as a function of control variables. During the numerical simulation, the transport equations are solved for these control variables together with fluid flow and state equations, while the thermochemical parameters are interpolated from the lookup table [30]. Through this preprocessing approach of combustion chemistry, the computational time is significantly reduced. Furthermore, due to the decoupled treatment

of the chemistry and fluid dynamics calculations, the chemical mechanism, at any level of detail, can be utilized.

In this study, the FGM lookup tables are generated using AVL TABKIN^{TM} table generation tool; see [31]. The FGM combustion model is based on a progress variable/mixture fraction approach. The progress variable is a scalar that varies between zero in fresh gas and unity in the burnt gas, subsequently representing progress in combustion reactions. Mixture fraction is a scalar that defines the mixing process in turbulent combustion. It is zero in the oxidizer and unity in the fuel. The mean general transport equation for the control variables can be described as follows:

$$\frac{\partial \overline{\rho}\widetilde{\phi}}{\partial t} + \frac{\partial \overline{\rho}\widetilde{u}_i\widetilde{\phi}}{\partial x_i} = \frac{\partial}{\partial x_i}\left(\overline{\rho}(D + D_T)\frac{\partial \widetilde{\phi}}{\partial x_i}\right) + \overline{\dot{\omega}_\phi} \tag{11}$$

where ϕ represents either the progress variable or mixture fraction. D and D_T are the laminar and turbulent diffusion coefficients of the fuel species. The subgrid coupling between turbulence and chemistry is based on a presumed probability density function (PDF) approach, applied to all control variables. More specifically, the lookup variables are averaged over the corresponding β-shape PDF as follows, assuming that the control variables are statistically independent:

$$\varnothing_{TCI}\left(y_1, \ldots, y_r, \widetilde{y}_1, \ldots, \widetilde{y}_r, y_1'', \ldots, y_r''\right) = \int \varnothing_{lam}(y_1, \ldots, y_r) \prod_{i=1}^{r} P_{\beta,i}\left(\widetilde{y}_i, y_i''\right) dy_i \tag{12}$$

where $P_{\beta,i}$ is the β-shaped presumed probability of the i-th control variable, as a function of its mean and its variance values. In this study, to consider the effects of sub-grid scales on the thermochemical state in the composition space, the statistical distribution of progress variable and mixture fraction is considered. The mean general transport equation for mixture fraction and progress variable variances is defined as follows:

$$\frac{\partial \overline{\rho}\widetilde{\phi}_{var}}{\partial t} + \frac{\partial \overline{\rho}\widetilde{u}_i\widetilde{\phi}_{var}}{\partial x_i} = \frac{\partial}{\partial x_i}\left(\overline{\rho}(D + D_T)\frac{\partial \widetilde{\phi}_{var}}{\partial x_i}\right) + 2\overline{\rho}D_T\left(\frac{\partial \widetilde{\phi}_{var}}{\partial x_i}\right)^2 - \overline{\rho}\widetilde{\chi}_\phi \tag{13}$$

$\widetilde{\chi}_\varnothing$ is a scalar dissipation rate defined by the following equation:

$$\widetilde{\chi}_\phi = 2\frac{\varepsilon}{k}\widetilde{\phi}_{var} \tag{14}$$

where, in the case of PANS simulation, k and ε are the unresolved turbulent kinetic energy and unresolved eddy dissipation rate. Commonly, in the premixed case, averaging is performed over the progress variable, and in the case of non-premixed application, it is performed over mixture fraction. Dual-fuel engines feature both premixed and non-premixed combustion regimes. Thus, in a dual-fuel configuration, the statistical distribution of both the progress variable and mixture fraction should be considered for accurate prediction of the species concentration and distribution. Additionally, the thermochemical effects of the second fuel have to be included in the lookup table. For that purpose, an additional dimension in terms of the fuel ratio or second mixture fraction is implemented to uniquely define the local dual-fuel composition. This scalar is defined as follows:

$$Fuel\ ratio := \frac{Z_{F1}}{Z_{F1} + Z_{F2}} \tag{15}$$

where Z_{F1} and Z_{F2} are the mixture fractions of premixed and non-premixed fuel, respectively.

The simultaneous consideration of premixed and non-premixed regimes in the single lookup table results in a substantial increase in the table size and the time required for table generation. Hence, the approach outlined in this work utilizes a dual-table configuration, with each table accounting for one combustion regime. To identify the dominant combus-

tion regime during the runtime, a scalar called the combustion regime indicator has been defined as follows:

$$CR := \frac{\chi_{PV}}{\chi_{PV} + \chi_Z} \tag{16}$$

where χ_{PV} and χ_Z are progress variable and mixture fraction dissipation rates. The combustion regime indicator is calculated during CDF simulation and, based on its value, the reactor solution is interpolated between two tables. In the premixed combustion regime, the combustion regime indicator holds a value of unity, while within the non-premixed regime, it is set at zero. Intermediate values indicate a partially premixed regime. In Figure 1, a schematic of the proposed approach is shown.

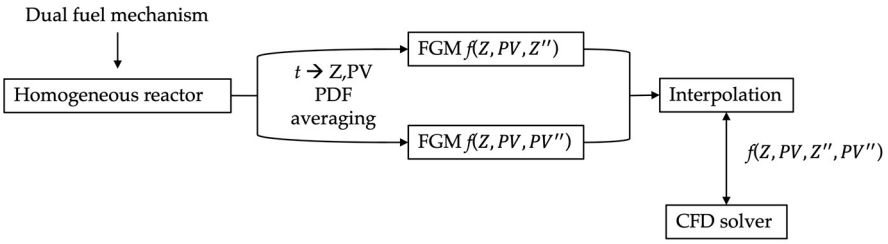

Figure 1. Schematic of the proposed dual-table approach.

In the following section, the feasibility of the proposed methodology is assessed in terms of memory and time requirements for table generation and solution interpolation, compared to a single-table approach that includes both regimes. Subsequently, the dual-table FGM combustion model is coupled with the PANS turbulence model to calculate the dual-fuel combustion process. The results are shown and discussed in Section 4.

2.3. FGM Dual-Table Approach Assessment

To test the feasibility of the proposed dual-table approach, chemical mechanisms with different levels of complexity were used to generate FGM lookup tables. The employed chemical mechanisms are summarized in Table 1.

Table 1. Employed chemical mechanisms.

Mechanism	Source	No. of Species/Reactions
NC7 V3	Lawrence Livermore National Laboratory [32]	654/2827
NC12	Lawrence Livermore National Laboratory [33]	223/1285
San Diego	University of California at San Diego [34]	69/301
TUW	Technical University of Vienna [12]	75/344
LLNL	Lawrence Livermore National Laboratory [35]	2885/11,754
TUG	Technical University of Graz [13]	190/334

For each mechanism, three tables are generated: one focusing solely on the premixed regime, another dedicated solely to the non-premixed regime, and a third accounting for both the premixed and non-premixed regimes. The AVL TABKIN^{TM} FGM combustion model has an additional available feature, namely the second progress variable, which transports slow chemistry processes such as nitrogen oxidation. Nevertheless, not every utilized chemical mechanism incorporates nitrogen reactions. As a result, the discretization of the tables varies based on whether or not the mechanism incorporates NO_x reactions. The chemical mechanisms that account for NO_x reactions are NC12, TUW and TUG, and for these mechanisms, the second progress variable has been adopted. The discretization of the lookup tables is given in Table 2. The pressure is discretized between 1 bar and 130 bar, and the temperatures are selected in the interval from 300 K to 2000 K. It should be noted that, regardless of the number of chemical species included in the chemical mechanism, the size of the resulting lookup table remains the same when using the same number of discretization points. Nevertheless, the computational runtime required to generate

the table increases as the number of species included in the mechanism increases. The tables were generated utilizing 20 compute nodes, each with two Intel® Xeon® Gold 6154 3.00 GHz processors containing 18 cores. In Table 3, a runtime comparison for tables generated without considering the second progress variable for different approaches to address turbulence chemistry interaction is shown. It is important to acknowledge that the last column of the table represents the cumulative generation time from two separate tables, each addressing the turbulent chemistry interaction solely over the progress variable or mixture fraction. Nevertheless, when sufficient computational power is available, these tables can be executed concurrently. In this scenario, the overall runtime aligns with the duration of the table that required more time for generation. The same comparison is made for the tables generated from the chemical mechanism that account for NO_x reaction and, therefore, the second progress variable is implemented. This comparison is given in Table 4.

Table 2. Table discretization for the mechanisms without NO_x reactions.

Dimension	No. of Discretization Points
Pressure	9
Temperature	17
Mixture fraction	56
Progress variable	110
Second progress variable *	110
Fuel ratio	6
Mixture fraction PDF	10
Progress variable PDF	12

* This dimension is only present in the tables generated from the mechanisms that consider NO_x reactions.

Table 3. Runtime overview for tables generated without second progress variable.

TCI	PV	Z	PV&Z	Dual Table
San Diego	2 h 3 min	1 h 36 min	12 h 4 min	3 h 39 min
NC7 V3	8 h 50 min	8 h 27 min	19 h 37 min	17 h 17 min
LLNL	2 days 1 h 9 min	2 days 49 min	6 days 1 h 16 min	4 days 1 h 58 min

Table 4. Runtime overview for tables with second progress variable.

TCI	PV	Z	PV&Z	Dual Table
TUW	2 h 28 min	1 h 48 min	21 h 15 min	4 h 16 min
NC12	3 h 22 min	2 h 44 min	26 h 34 min	6 h 6 min
TUG	3 h 24 min	2 h 34 min	29 h 27 min	5 h 58 min

As evident from the shown cases, the simultaneous incorporation of the progress variable and mixture fraction variances within the same table necessitates a longer generation time, in contrast to the approach involving the creation of two distinct tables and subsequent interpolation of reactor solutions from them. Moreover, the time required to generate a single table encompassing both progress variable and mixture fraction variances is greater than the time needed to generate two separate tables, each addressing a single variance in sequence. This disparity would be even more pronounced if the number of discretization points was increased.

Furthermore, when both the progress variable and mixture fraction variances are simultaneously accounted for, the resulting table size is approximately five times larger than the memory requirement for two separate tables. This observation holds true for scenarios both with and without the inclusion of the second progress variable. The sizes of the resulting tables are illustrated in Table 5.

Table 5. Memory size (GB) of the lookup tables with different TCI approximations.

TCI	PV	Z	PV&Z	Dual Table
No 2nd PV	4.8	3.9	44	8.7
With 2nd PV	12	9.3	109	21.3

This test has been conducted to underline the necessity for an innovative methodology within the FGM combustion model that efficiently considers turbulence–chemistry interactions across both the progress variable and mixture fraction. The primary objective of this investigation is to introduce an efficient numerical simulation workflow tailored for the advancement and design of dual-fuel IC engines applicable in routine industrial operations. For that purpose, a dual-table FGM combustion modeling approach has been coupled with a PANS $k-\zeta-f$ turbulence model. The ensuing performance of this methodology is subsequently validated against accessible experimental data pertaining to the combustion process in dual-fuel internal combustion engines. Detailed results and discussions are presented in Section 4.

3. Validation of the Proposed Numerical Methodology

In this section, the validation of the proposed numerical methodology for simulating dual-fuel combustion processes, as previously discussed, is elaborated. First, the experimental setup is introduced followed by an elaboration on the chosen validation cases. Finally, the numerical setup is explained.

3.1. Experimental Setup

To validate the proposed numerical methodology, experimental data obtained from the Large Engine Competence Center in Graz were used. A large, high-speed, single-cylinder research engine was used in the experimental campaign to obtain data on the dual-fuel combustion process. The main engine specifications are given in Table 6. The focus of this investigation is a so-called diesel ignited gas engine. The concept employs a lean, homogeneous mixture of air and natural gas, introduced into the combustion chamber via port injection or central mixture formation. Subsequently, a small quantity of diesel fuel, serving as an ignition source, is injected into the combustion chamber. This initiates the combustion of the surrounding mixture, which means that the autoignition of the diesel fuel is followed by premixed combustion of the background mixture [4]. The diesel fuel was injected with a four-hole injector nozzle with a common rail system [7].

Table 6. SCE technical details [7].

Engine speed	1500 rpm
Stroke/Bore	220/190 mm
Connecting rod	425 mm
Compression ratio	12:1
Swirl/tumble	0/0
Displacement	6.24 dm^3
Number of inlet/exhaust valves	2/2
Charge air	Provided by an external compressor with up to 10 bar boost pressure
Gas fuel supply	External mixture formation via a venturi mixer
Diesel fuel supply	Common rail system with up to 1600 bar rail pressure

In the context of this study, three distinct representative operating conditions have been chosen, each differing in the injection timing of the pilot diesel fuel. The injection timing was adjusted by -10° CA and $+10^\circ$ CA relative to the nominal operating point. The work of Redtenbacher et al. [5] has revealed that varying the injection timing, even at modest diesel fractions such as 1%, can result in significant variations in combustion characteristics. As such, the chosen operating points offer a robust foundation for investigating the dual-fuel

combustion process. A summary of parameters for the selected operating conditions is provided in Table 7.

Table 7. Selected engine operating conditions.

Diesel fraction	1.5%
Global lambda	1.7
IMEP	24 bar
Intake charge temperature	318 K
Diesel injection timing	Early, middle, late

3.2. Numerical Setup

All 3D-CFD simulations were conducted using the commercial 3D-CFD code AVL FIRE^{TM}. The code employs a fully conservative finite volume approach, based on the integral form of the general conservation law applied to unstructured moving grids composed of arbitrary polyhedral elements. Dependent variables are evaluated at the center of each control volume. To accommodate an arbitrary number of cell faces, cell-face-based connectivity and interpolation techniques for gradients and face values are introduced. A second-order midpoint rule is used for integral approximation and second-order linear approximation is used for any value at the call face. Integral approximation rests on a second-order midpoint rule, while a second-order linear approximation is applied for values at cell faces. After employing special interpolation practices, a diffusion term is incorporated into the surface integral source. Various differencing schemes are employed for solving convection. For turbulence and energy transport equations, a first-order upwind differencing scheme is employed, while the continuity equation is discretized by a central differencing scheme. The momentum equation is discretized using the MINMOD relaxed scheme. The time derivatives are discretized employing the first-order Euler implicit scheme. The overall solution is iterative, and it is based on the Semi-Implicit Method for Pressure-Linked Equations (SIMPLE) algorithm [36]. The PANS model is used in conjunction with hybrid wall treatment [37], a method that combines integration up to the wall with the wall functions, enabling well-defined boundary conditions regardless of the position of the wall adjacent numerical node.

The computational mesh is generated for only one-fourth of the cylinder since the diesel injector has four symmetrically arranged nozzle holes. Only a high-pressure phase was simulated. The computational domain is shown in Figure 2. The employed computational mesh is chosen based on the mesh dependency study conducted in [22]. The mesh consists of hexahedral elements with the number of cells in the mesh being 389,125 and 2,314,750 at the top dead center and bottom dead center, respectively. A moving, constant temperature wall boundary condition is applied to the piston surface, while the constant temperature condition is prescribed for the cylinder head selection. A periodic boundary condition was applied to both sides of the domain since the cylinder geometry was assumed to be symmetric around the cylinder axis. The initial conditions are defined according to experimental data given in Tables 6 and 7.

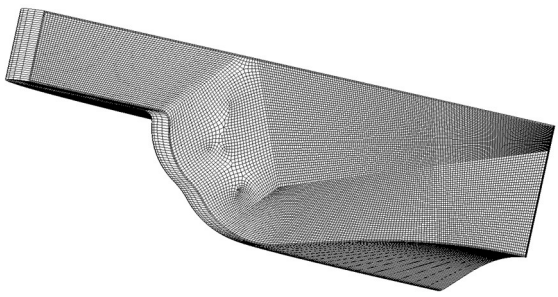

Figure 2. Computational mesh used in simulation.

Injection Modeling

Accurate modeling of the diesel injection process is important in order to understand the spray formation, its interaction with surrounding air in the cylinder and the location where diesel will ignite, and to achieve more efficient and complete combustion followed by lower pollutant emissions [22]. The most common method for numerical modeling of the spray process for engineering calculations is based on the Discrete Droplet Model (DDM), where the liquid phase is described by Lagrangian particles, while the gas phase is modeled in the Eulerian framework [38]. Despite several shortcomings, this method has demonstrated its efficiency and sufficient accuracy in predicting spray dynamics in the industrial development process. Therefore, in this study, DDM has been coupled with the dual-table FGM combustion model and the PANS $k - \zeta - f$ turbulence model to simulate the dual-fuel combustion process. Eder et al. [4,7] optimized and calibrated the spray model parameters based on the optical measurements of injection sprays in an inert atmosphere. Under dual-fuel operation, the needle primarily functions in a ballistic mode, which results in a relatively low initial velocity. To tackle this challenge, Eder et al. [7] introduced a non-constant nozzle hole diameter that mirrors the shape of the rate of injection, as illustrated in Figure 3. Furthermore, the nozzle diameter is adjusted to prevent velocities from surpassing the maximum achievable limit. These adaptations enabled the consideration of the ballistic region of the needle lift. The initial velocity from the 3D-CFD simulation is depicted in Figure 4. A set of spray sub-models has been employed to account for primary and secondary break-up processes, evaporation, wall interaction and turbulent dispersion. These sub-models include the WAVE break-up model, the Dukowicz evaporation model, and the Walljet wall interaction model; see [39]. Resolving the impact of turbulence on spray particles is infeasible; thus, it is addressed through the implementation of a turbulent dispersion model. In the case of the PANS simulation, the turbulent dispersion model considers the interaction between resolved flow scales and the spray droplets.

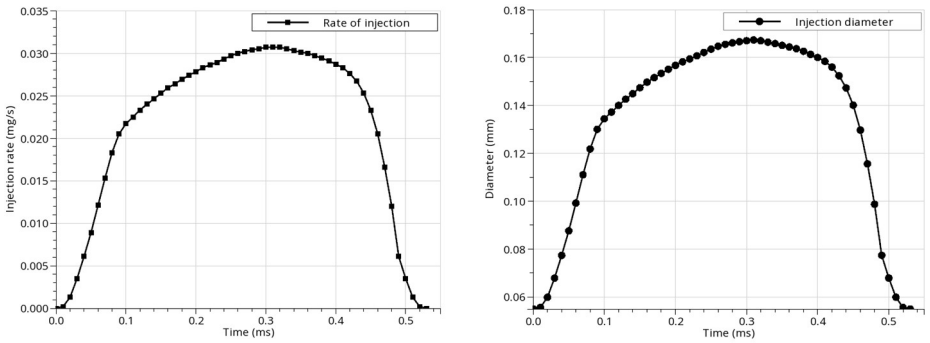

Figure 3. (**a**) Rate of injection curve and (**b**) modified nozzle hole diameter with non-constant value.

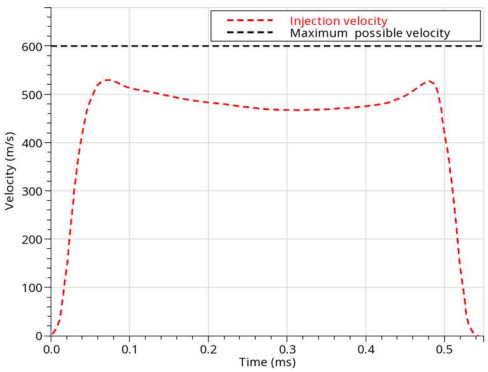

Figure 4. Injection velocity from 3D-CFD simulation.

4. Results and Discussion

In order to highlight the advantages of the FGM combustion modeling approach in terms of computational efficiency, comparisons were made between FGM simulations and detailed chemistry simulations employing a detailed diesel surrogate chemical kinetics mechanism developed by the Lawrence Livermore National Laboratory (LLNL). This mechanism describes the oxidation of an n-dodecane/m-xylene mixture and incorporates 2885 species and 11,754 elementary reactions [35]. The numerical results are validated against experimental in-cylinder pressure traces and the rate of heat release curves for three engine operating points.

As a first step, in Figure 5, a comparison is made between the temperature curves obtained from a 0D calculation using the LLNL chemical mechanism and those from a 3D CFD simulation employing the FGM dual-table combustion modeling approach, utilizing tables generated from the same chemical mechanism. The CFD simulation utilized a straightforward cubic domain comprising 50 hexahedral cells. The results reveal that the ignition delay time from the CFD simulation closely aligns with the ignition delay time determined through the 0D calculation. This congruence suggests that the accuracy of predicting the ignition delay time is maintained even in the presence of chemistry tabulation.

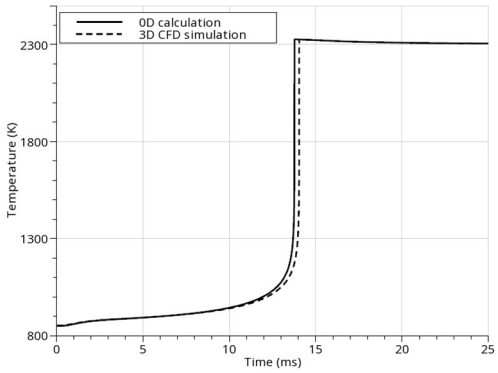

Figure 5. Comparison of the ignition delay time obtained from 0D calculation and 3D CFD simulation with tabulated chemistry for p = 55 bar and T = 850 K.

Figure 6 illustrates the results of the 0D perfectly stirred reactor (PSR) simulation using the LLNL chemical kinetics mechanism. The simulations were conducted for a fuel ratio of zero, representing pure diesel, and a fuel ratio of 0.8, corresponding to a dual-fuel mixture with 80% methane content. The conditions for both cases were a temperature of 850 K and a pressure of 55 bar. The progress variable source term is mapped onto a predefined progress variable and mixture fraction grid.

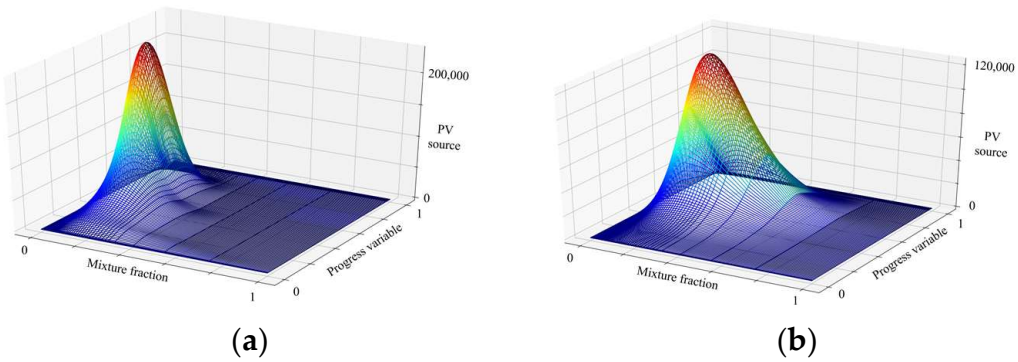

Figure 6. Progress variable source term as a function of progress variable and mixture fraction, at p = 55 bar and T = 850 K for a fuel ratio of (**a**) 0 and (**b**) 0.8.

The results indicate that the distribution of the progress variable source is similar for both cases, but the peak values attained for the dual-fuel mixture are lower. Additionally, in both cases, the progress variable source term has its maximum at the stoichiometric mixture fraction. As previously mentioned, the presence of premixed gaseous fuel alters the mixture formation and, consequently, the combustion characteristics of the pilot diesel fuel. Specifically, in this case, methane significantly extends the ignition delay time of diesel fuel. This phenomenon is well-known, having been confirmed both experimentally and numerically. This behavior is further evident in Figure 7, which depicts the progress variable source plotted against the fuel ratio. As the methane content increases in the dual-fuel mixture, the progress variable source term decreases and consequently prolongs the ignition delay time. To provide an accurate description of the autoignition of the dual-fuel mixture, it is crucial to represent both fuels—methane and diesel—in the reaction chemistry. It is evident that the thermochemical effects of the second fuel are at the very least qualitatively correctly captured within the FGM lookup tables.

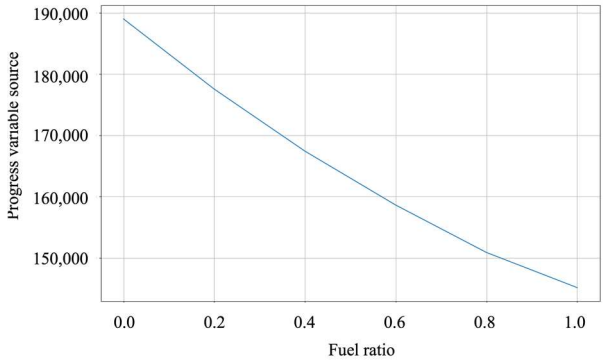

Figure 7. Progress variable source term as a function of the fuel ratio.

In addition, Figures 8 and 9 visualize the output of 0D PSR simulations for a table boundary temperature of 1250 K for the pure diesel case and dual-fuel configuration with an 80% methane content. In these figures, the CO_2 and soot mass fraction are mapped on a predefined progress variable and mixture fraction grid, respectively. The results demonstrate an already proven trend [40]: the introduction of gaseous fuel leads to a reduction in both CO_2 and soot mass fractions. Notably, the peak values occur at a mixture fraction approximately corresponding to the stoichiometric mixture value. Over the years, there has been significant research into the nature and extent of exhaust emissions from dual-fuel engines. Dual-fuel-type compression ignition engines, fueled with various gaseous fuel resources, produce less exhaust emissions than conventional diesel engines without any substantial operating and capital costs [40]. The tabulated chemistry approach has demonstrated its ability to preserve the inherent characteristics of species formation from the chemical kinetics mechanism.

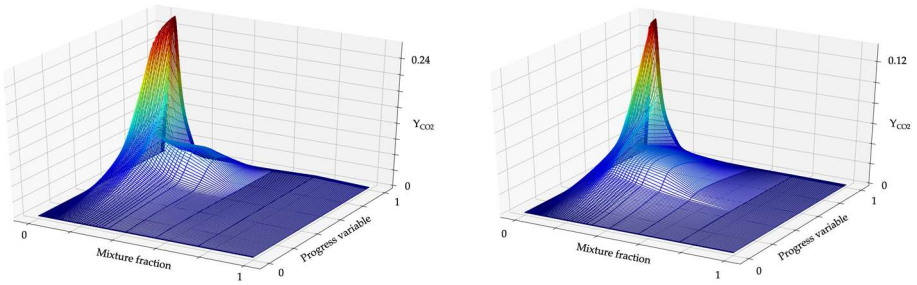

Figure 8. CO_2 mass fraction as a function of the mixture fraction and progress variable at a temperature of 1250 K for a fuel ratio of (**a**) 0 and (**b**) 0.8.

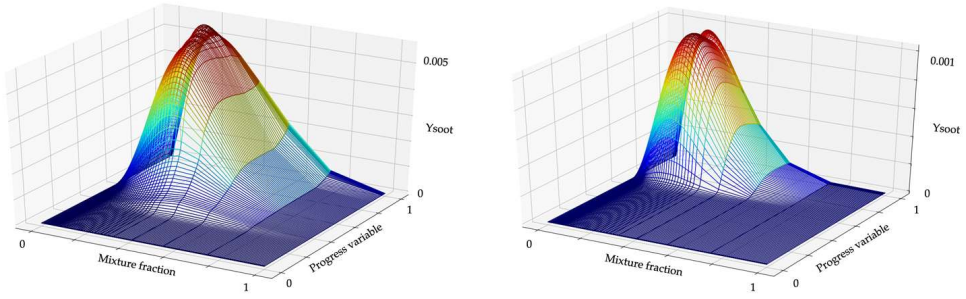

(**a**) (**b**)

Figure 9. Soot mass fraction as a function of the mixture fraction and progress variable at a temperature of 1250 K for a fuel ratio of (**a**) 0 and (**b**) 0.8.

In Figures 10–12, the in-cylinder pressure traces and rate of heat release curves are presented, which were obtained from 3D CFD simulations, utilizing the FGM combustion model and employing distinct approaches to consider turbulence chemistry interactions. The results are validated against experimental results from the single-cylinder, dual-fuel research engine described in Section 3. The same trend is consistently observed across all three engine operating points. When only the progress variable variance is taken into consideration, the combustion process starts too early, and the peak from the premixed combustion and peak pressure values are overpredicted. On the other hand, when only mixture fraction variance is considered, all of the values are significantly underpredicted, resulting in incomplete fuel combustion. Simulations where the reactor solution is interpolated from both tables align well with experimental data in terms of peak values and the onset of combustion. This concordance indicates that, for an accurate depiction of the dual-fuel combustion process, it is essential to account for both premixed and non-premixed combustion regimes. Furthermore, the presented results indicate that the dual-table FGM combustion modeling approach, which accounts for different combustion regimes through PDF averaging of control variables, holds potential for accurately predicting the dual-fuel combustion process. This approach also demonstrates the advantage of lower computational costs in comparison to the single-table approach that attempts to simultaneously consider both regimes.

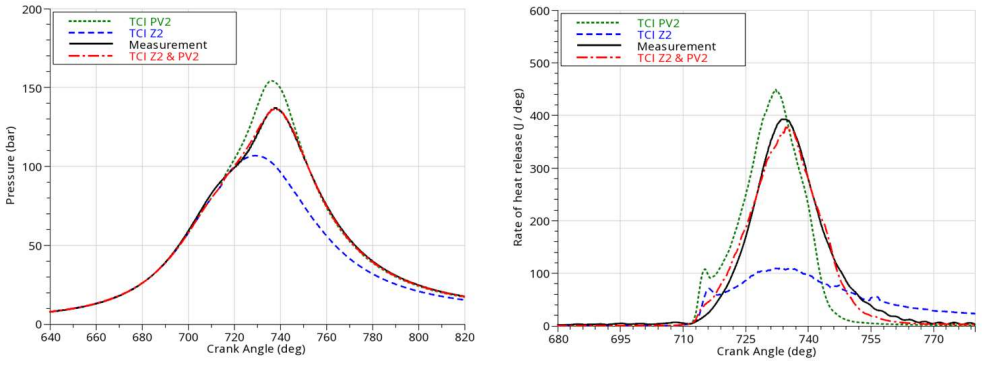

(**a**) (**b**)

Figure 10. Comparison of (**a**) in-cylinder pressure and (**b**) rate of heat release as obtained using FGM simulation with different turbulent chemistry interaction treatments for early injection engine operating point.

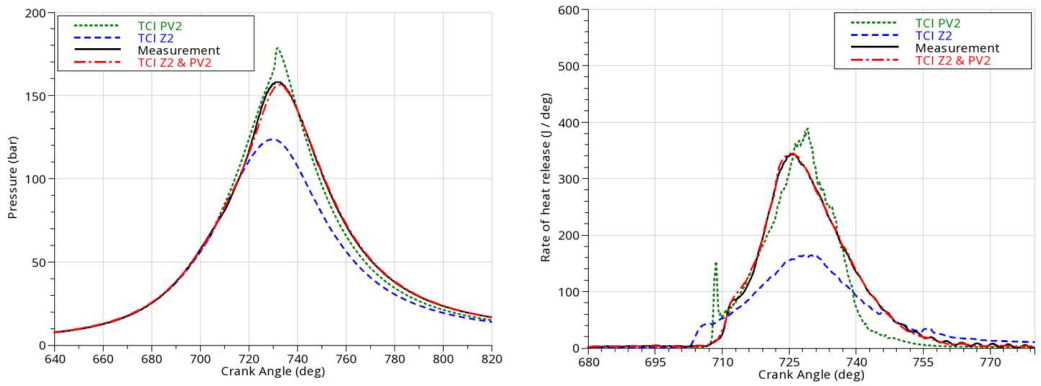

Figure 11. Comparison of (**a**) in-cylinder pressure and (**b**) rate of heat release as obtained using FGM simulations with different turbulent chemistry interaction treatments for middle injection engine operating point.

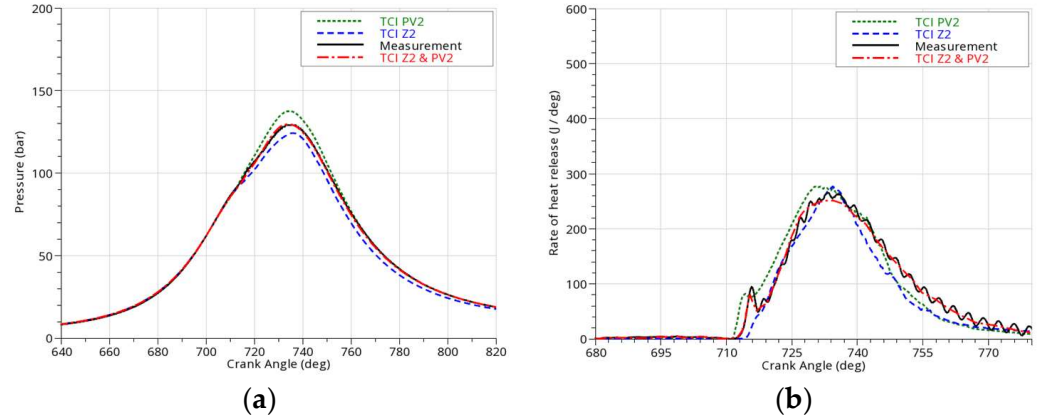

Figure 12. Comparison of (**a**) in-cylinder pressure and (**b**) rate of heat release as obtained using FGM simulations with different turbulent chemistry interaction treatments for late injection engine operating point.

As stated previously, the principal aim of this study is to propose an optimal numerical simulation workflow for designing dual-fuel IC engines and their associated injection systems, tailored for everyday industrial applications. Therefore, the dual-table FGM combustion modeling approach has been coupled with the PANS $k-\zeta-f$ turbulence model. The work presented in [22] has already demonstrated the potential of the PANS $k-\zeta-f$ turbulence model to accurately predict the dual-fuel combustion process with reduced computational demands, as compared to the approach in which the LES turbulence modeling approach is employed. Moreover, the same study highlighted the PANS $k-\zeta-f$ model's capability to predict cycle-to-cycle variations. Following this, a similar study has been performed in this work. For the late injection engine operating point, the dual-fuel combustion process is simulated using three distinct turbulence modeling approaches coupled with the dual-table FGM combustion model: the RANS $k-\zeta-f$ model, PANS $k-\zeta-f$ model, and the LES-with-subgrid model based on the coherent structure function as developed by Kobayashi [41,42]. Figure 13 shows the comparison of temperature and velocity fields as obtained with these different turbulence modeling methods, all on the same computational mesh. Observing the results, it becomes evident that RANS simulation results are very smooth, with no visible fluctuations or small-scale structures. In contrast, PANS results show more pronounced wrinkle-like patterns due to resolving the portion of the turbulent flow scales. When comparing the PANS results and LES results on the same mesh, it becomes apparent that PANS yields an equivalent level of detail in terms of resolving a portion of fluctuating flow scales. However, a noteworthy distinction arises:

the PANS simulation shows more accurate prediction than the LES simulation in the near-wall region. This can be attributed to the fact that the PANS model can be effectively coupled with the universal wall approach, which combines the integration up to the wall with the wall functions. In contrast, for wall-resolved LES calculation, a very fine numerical grid is needed, and most industrial computations cannot meet this stringent requirement [27]. Based on the results, it can be concluded that the employed numerical mesh resolution is inadequate to accurately capture the involved physical phenomena with the LES CSM model.

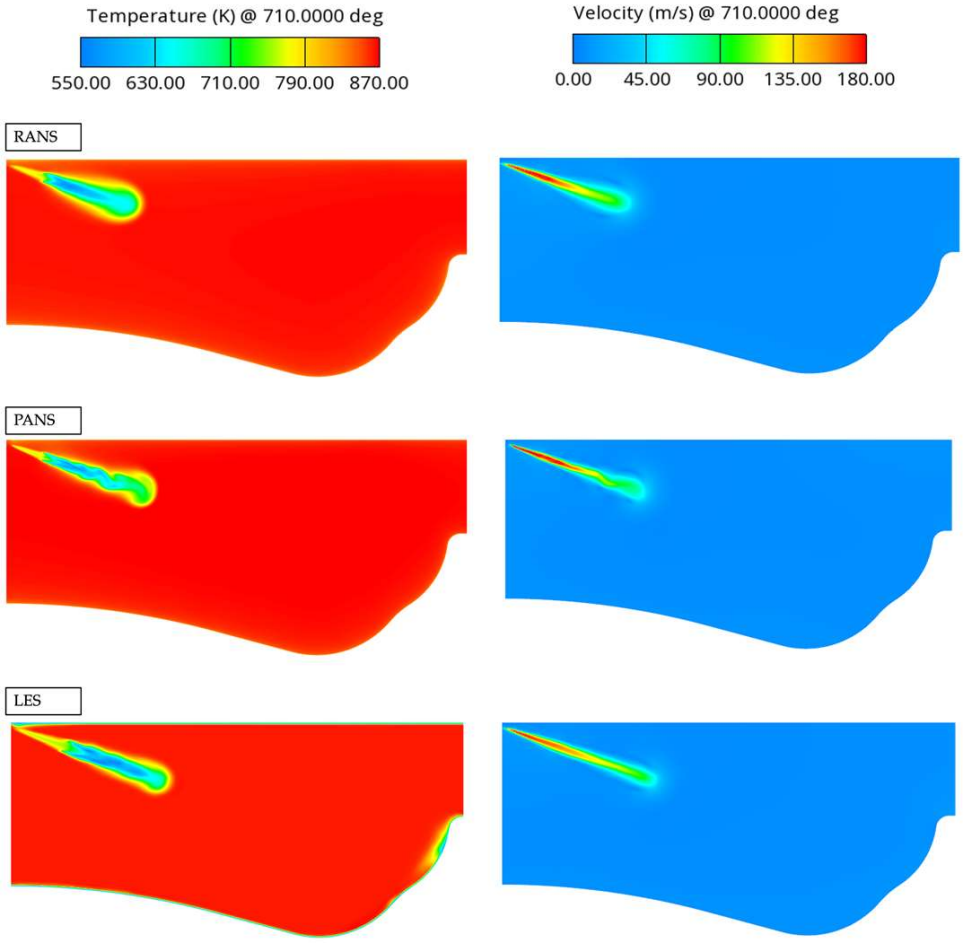

Figure 13. Comparison of the temperature (**left**) and velocity (**right**) fields as obtained using 3D CFD simulations employing a RANS $k-\zeta-f$ turbulence model (**upper** row), PANS $k-\zeta-f$ turbulence model (**middle** row) and LES CSM turbulence model (**lower** row).

Figure 14 illustrates the PANS model's resolution parameter along with the total, resolved or SSV turbulence, as well as the unresolved turbulent kinetic energy. Notably, the highest value of the resolution parameter is found near the nozzle exit, signifying that this portion of the flow remains beyond the resolution capability of the employed mesh. Furthermore, it is worth mentioning that the resolution parameter values are notably below unity in the central part of the cylinder and equal to unity near the wall. Consequently, within regions where the resolution parameter equals unity, the PANS model transitions to its RANS parent model, leading to a completely modeling turbulent flow. This ensures an adequate description of in-cylinder processes, even in the cases where the mesh resolution is insufficient for resolved simulation in those areas. Correspondingly, the maximum unresolved turbulent kinetic energy is situated in regions where the resolution parameter exhibits higher values. In contrast, the maximum resolved energy is found in areas where

the resolution parameter has lower values. The total turbulent kinetic energy is obtained by summing the resolved and unresolved turbulent kinetic energy components.

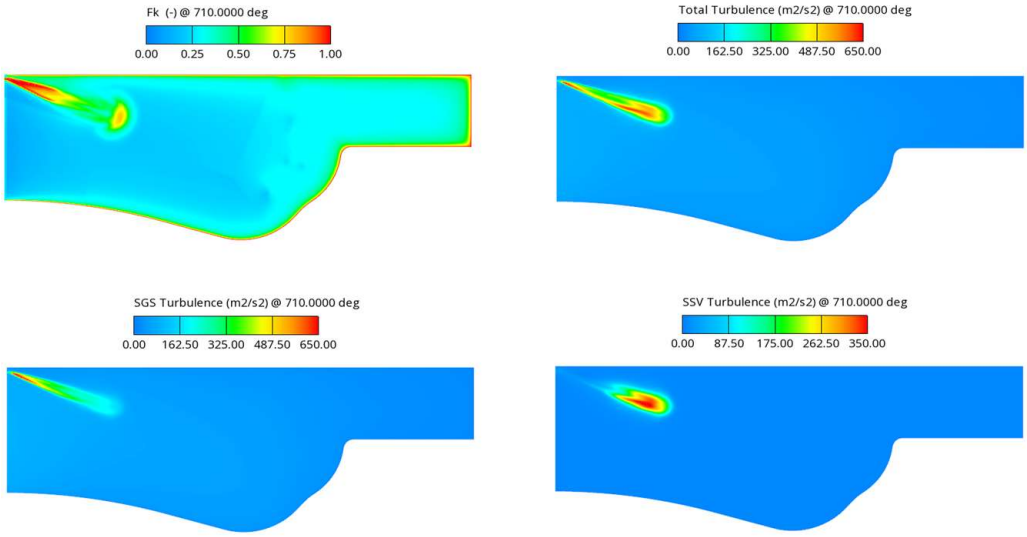

Figure 14. The PANS model resolution parameter (**upper left**), total turbulent kinetic energy (**upper right**), unresolved turbulent kinetic energy (**lower left**), and resolved turbulent kinetic energy (**lower right**).

Finally, the following instantaneous pictures in Figure 15 illustrate the relationship between the combustion regime indicator and the mass fraction of evaporated pilot fuel, as obtained using a dual-table FGM PANS simulation approach. Evidently, this demonstrates that the implemented combustion regime indicator is capable of distinguishing the premixed, non-premixed, and partially premixed regions within the domain. It is worth noting that this scalar accounts solely for the gaseous phase of the mixture fraction, transitioning to the partially premixed regime only when the spray starts to evaporate.

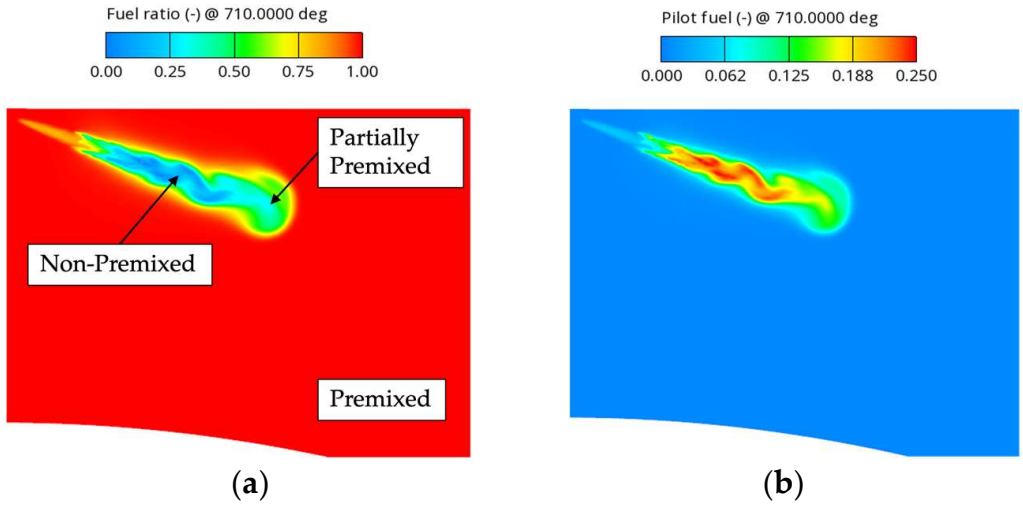

Figure 15. Instantaneous distribution of combustion (**a**) regime indicator and (**b**) evaporated pilot fuel mixture fraction.

Up to this point, the dual-table FGM combustion modeling approach has effectively demonstrated its capacity to accurately capture the thermochemical impacts of the chemical kinetics mechanism. Notably, the dual-table approach has proven to be computationally less demanding compared to the single-table approach. Moreover, the PANS turbulence model has exhibited its potential to yield a more detailed solution compared to RANS, on coarser meshes that are typically not sufficient for LES requirements. Hence, this simulation workflow has been employed to simulate another important aspect of the IC engine, namely cycle-to-cycle variations. In order to perform this numerical study on cyclic variations, initial and boundary conditions were perturbed based on the work of [43–45]. This test is mainly performed to investigate the feasibility of the dual-table FGM PANS modeling approach to predict cycle-to-cycle variations compared to detailed chemistry simulation in terms of the computational cost and accuracy. In this study, thirty individual cycles were simulated in parallel on 90-degree sector mesh utilizing 60 CPUs. The outcome of this study is shown in Figure 16. It is evident from the presented results that numerically obtained pressure traces lie in the range of the experimentally measured minimum and maximum in-cylinder pressure. It is evident from Figure 17 that the numerically obtained pressure trace and rate of heat release averaged over 30 cycles are in good agreement with the average pressure trace and rate of heat release from the measurement. In the same figure, a pressure trace and rate of heat release as obtained using detailed chemistry simulation coupled with a PANS turbulence model are shown. Detailed chemistry simulation is performed utilizing the same chemical kinetics mechanism, namely the previously mentioned LLNL, on the same numerical mesh utilizing 60 CPUs. The solver turnaround time for one high-pressure phase combustion cycle on 90-degree sector mesh for detailed chemistry simulation is 77 days. Performing the multicycle simulation utilizing a detailed chemistry approach was unfeasible; therefore, the required computational time can only be estimated. The computational time required for FGM and detailed chemistry simulation are compared in Table 8. The FGM tables have to be generated prior to the CFD simulation, and then the same table is used for every cycle. It is evident from the presented results that the FGM combustion modeling approach enables a substantial reduction in the computational time compared to detailed chemistry simulation.

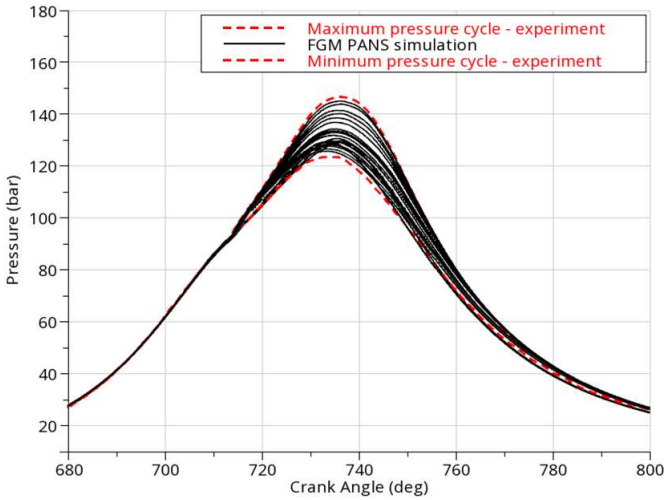

Figure 16. Cycle-to-cycle in-cylinder pressure variations as predicted by dual-table FGM PANS simulation methodology.

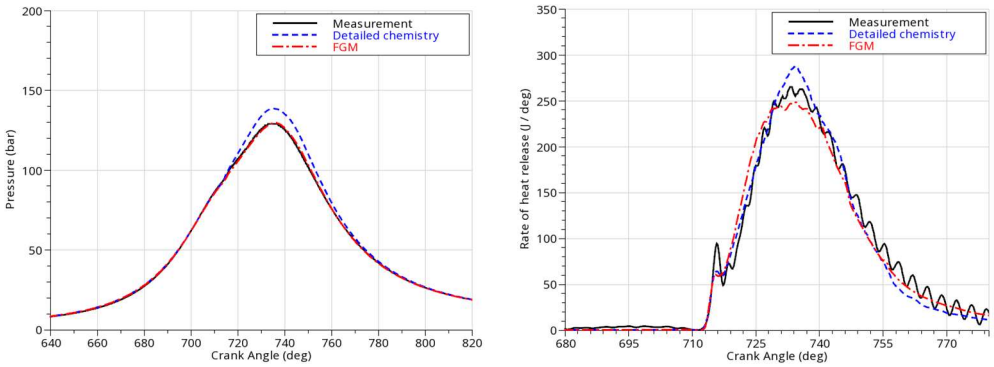

Figure 17. (**a**) Average pressure trace and (**b**) rate of heat release as obtained from dual-table FGM PANS simulation compared to one-cycle detailed chemistry simulation and measurement.

Table 8. Computational time required for the multiple cycle simulation of dual-fuel combustion utilizing FGM and detailed chemistry simulation approach.

	FGM	Detailed Chemistry
Table generation	4 days 1 h 58 min	/
Solver per case	23 h	77 days
Solver for 30 cycles	28 days 45 min	...

5. Conclusions

The focus of the present study was to establish an optimal 3D CFD simulation workflow for the design of a diesel ignited gas internal combustion engine. For this purpose, a novel cost-effective methodology for handling multiple fuels within a flamelet-generated manifold tabulated chemistry combustion modeling approach was introduced. Accurate simulation of dual-fuel combustion processes requires modeling of both premixed and non-premixed combustion regimes. However, attempting to incorporate both regimes into a single FGM lookup table significantly increases the table size and generation time. In response, the approach proposed in this work adopts a dual-table configuration, with each table tailored to a specific combustion regime. The solution is then interpolated from these tables based on the combustion regime indicator, calculated during 3D CFD simulation. The validation of this methodology is performed utilizing six chemical kinetics mechanisms with different levels of detail. For each mechanism, three tables are generated: one focusing solely on the premixed regime, another focusing solely on the non-premixed regime, and a third considering both the premixed and non-premixed regimes. This strategy has been shown to optimize the computational efficiency while preserving precision in dual-fuel combustion representation. To establish a cost-effective and more detailed 3D CFD simulation workflow, the dual-table FGM methodology is coupled with the partially averaged Navier–Stokes turbulence model. Employing the PANS model for turbulence, the unsteady flow features are captured more accurately compared to the conventional RANS modeling approach with fewer computational cells than required for LES. Finally, the proposed FGM PANS methodology demonstrated its potential to accurately predict the combustion process in a dual-fuel engine for three engine operating points with significantly lower computational requirements compared to detailed chemistry simulation.

Author Contributions: M.S. conducted simulations, performed data analysis and prepared the manuscript. B.B., S.J.S. and N.A.A. proofread the manuscript, provided guidance on the research direction and supervised the work. B.B. provided funding and software support. All authors have read and agreed to the published version of the manuscript.

Funding: This work has received funding from the European Union's Horizon 2020 research and innovation programme under Marie Sklodowska-Curie grant agreement No. 861002.

Data Availability Statement: Data are contained within the article.

Conflicts of Interest: Authors Branislav Basara and Marija Stipic were employed by the company AVL List GmbH. The remaining authors declare that the research was conducted in the absence of any commercial or financial relationships that could be construed as a potential conflict of interest.

Abbreviations

Symbols	
D	Laminar diffusion coefficient of species i (m^2/s)
D_T	Turbulent diffusion coefficient of species i (m^2/s)
f	Elliptic relaxation function
f_k	Unresolved to total turbulent kinetic energy ratio (-)
f_ε	Unresolved to total eddy dissipation ratio (-)
k	Turbulent kinetic energy (m^2/s^2)
k_r	Resolved turbulent kinetic energy (m^2/s^2)
k_u	Unresolved turbulent kinetic energy (m^2/s^2)
k_{ssv}	Scale supplying variable (m^2/s^2)
k_{tot}	Total turbulent kinetic energy (m^2/s^2)
T	Temperature (K)
t	Time (s)
P	Partially filtered pressure component (Pa)
p	Instantaneous pressure field (Pa)
p'	Unresolved pressure component (Pa)
U_i	Partially filtered velocity component in the direction i (m/s)
u_i	Unresolved velocity component in the direction i (m/s)
V_i	Instantaneous velocity component in the direction i (m/s)
y_i	Species mass fraction (-)
δ_{ij}	Kronecker delta
Δ	Mesh size (m)
ε_u	Unresolved eddy dissipation rate (m^2/s^3)
ν_u	Turbulent eddy viscosity (m^2/s)
ρ	Density (kg/m^3)
Λ	Integral length scale (m)
ζ	Velocity scale ratio (-)
τ	Viscous stress tensor (N/m^2)
χ	Scale dissipation rate (-)
Abbreviations	
3D-CFD	Three-dimensional computational fluid dynamics
CA	Crank angle
CCV	Cycle-to-cycle variation
DF	Dual fuel
DFICE	Dual-fuel internal combustion engine
DNS	Direct numerical simulation
FGM	Flamelet-generated manifold
ICE	Internal combustion engine
LEC	Large engine competence center
LES CSM	Large eddy simulation coherent structure model
PANS	Partially averaged Navier–Stokes
PDF	Probability density function
PSR	Perfectly stirred reactor
RANS	Reynolds-averaged Navier–Stokes
SSV	Scale supplying variable
TCI	Turbulent chemistry interactions

References

1. *World Population Prospects 2022 Summary of Results*; United Nations Department of Economic and Social Affairs, Population Division: New York, NY, USA, 2022.
2. Teter, J.; Cazzola, P.; Gul, T.; Mulholland, E.; Le Feuvre, P.; Bennett, S.; Hugues, P.; Lagarde, Z.; Kraayvanger, V.; Bryant, T.; et al. *The Future of Trucks Implications for Energy and the Environment*, 2nd ed.; International Energy Agency: Paris, France, 2017.
3. Karim, G.A. *Dual-Fuel Diesel Engines*; CRC Press: Boca Raton, FL, USA, 2015. [CrossRef]
4. Eder, L.; Kiesling, C.; Priesching, P.; Pirker, G.; Wimmer, A. *Multidimensional Modeling of Injection and Combustion Phenomena in a Diesel Ignited Gas Engine*; SAE Technical Papers; SAE International: Detroit, MI, USA, 2017. [CrossRef]
5. Redtenbacher, C.; Kiesling, C.; Malin, M.; Wimmer, A.; Pastor, J.V.; Pinotti, M. Potential and Limitations of Dual Fuel Operation of High Speed Large Engines. *J. Energy Resour. Technol.* **2018**, *140*, 032205. [CrossRef]
6. Veynante, D.; Vervisch, L. Turbulent combustion modeling. *Prog. Energy Combust. Sci.* **2002**, *28*, 193–266. [CrossRef]
7. Eder, L.; Ban, M.; Pirker, G.; Vujanovic, M.; Priesching, P.; Wimmer, A. Development and validation of 3D-CFD injection and combustion models for dual fuel combustion in diesel ignited large gas engines. *Energies* **2018**, *11*, 643. [CrossRef]
8. Liu, Z.; Karim, G.A. Simulation of combustion processes in gas-fuelled diesel engines. *Proc. Inst. Mech. Eng. Part A J. Power Energy* **1997**, *211*, 159–169. [CrossRef]
9. Schlatter, S.; Schneider, B.; Wright, Y.; Boulouchos, K. *Experimental Study of Ignition and Combustion Characteristics of a Diesel Pilot Spray in a Lean Premixed Methane/Air Charge Using a Rapid Compression Expansion Machine*; SAE Technical Papers; SAE International: Detroit, MI, USA, 2012. [CrossRef]
10. Aggarwal, S.K.; Awomolo, O.; Akber, K. Ignition characteristics of heptane–hydrogen and heptane–methane fuel blends at elevated pressures. *Int. J. Hydrogen Energy* **2011**, *36*, 15392–15402. [CrossRef]
11. Hockett, A.; Hampson, G.; Marchese, A.J. Development and Validation of a Reduced Chemical Kinetic Mechanism for Computational Fluid Dynamics Simulations of Natural Gas/Diesel Dual-Fuel Engines. *Energy Fuels* **2016**, *30*, 2414–2427. [CrossRef]
12. Schuh, S.; Frühhaber, J.; Lauer, T.; Winter, F. A novel dual fuel reaction mechanism for ignition in natural gas–diesel combustion. *Energies* **2019**, *12*, 4396. [CrossRef]
13. Eder, L. Entwicklung und Validierung von 3D-CFD Verbrennungsmodellen für die Simulation von Großgasmotoren mit Pilotölzündung. Ph.D. Thesis, Technical University of Graz, Graz, Austria, 2018.
14. Priesching, P.; Tvrdojevic, M.; Tap, F.; Meijer, C. *Prediction of the Combustion and Emission Processes in Diesel Engines Based on a Tabulated Chemistry Approach*; SAE Technical Papers; SAE International: Detroit, MI, USA, 2017. [CrossRef]
15. Tvrdojevic, M.; Vujanovic, M.; Priesching, P.; Tap, F.A.; Starikov, A.; Goryntsev, D.; Gavaises, M. Implementation of the Semi Empirical Kinetic Soot Model within Chemistry Tabulation Framework for Efficient Emissions Predictions in Diesel Engines. *Open Phys.* **2020**, *17*, 905–915. [CrossRef]
16. Goryntsev, D.; Tap, F.; Tvrdojevic, M.; Priesching, P. *SI Engine Combustion and Knock Modelling Using Detailed Fuel Surrogate Models and Tabulated Chemistry*; SAE Technical Papers; SAE International: Detroit, MI, USA, 2019. [CrossRef]
17. Jakirlic, S.; Kutej, L.; Basara, B.; Tropea, C. Computational Study of the Aerodynamics of a Realistic Car Model by Means of RANS and Hybrid RANS/LES Approaches. *SAE Int. J. Passeng. Cars Mech. Syst.* **2014**, *7*, 2014-01. [CrossRef]
18. Chang, C.Y.; Krumbein, B.; Bopp, M.; Basara, B.; Sadiki, A.; Hasse, C.; Dreizler, A.; Boehm, B.; Jakirlic, S. *Structural Flow Properties in IC Engine-Relevant Piston-Cylinder Configurations: An Eddy-Resolving Modelling Study*; SAE Technical Papers; SAE International: Detroit, MI, USA, 2022. [CrossRef]
19. Rutland, C.J. Large-eddy simulations for internal combustion engines—A review. *Int. J. Engine Res.* **2011**, *12*, 421–451. [CrossRef]
20. Basara, B.; Krajnović, S.; Girimaji, S. PANS vs. LES for computations of the flow around a 3D bluff body. In Proceedings of the 7th International ERCOFTAC Symposium on Engineering Turbulence Modelling and Measurements (ETMM-7), Lymassol, Cyprus, 4–8 June 2008.
21. Basara, B.; Girimaji, S.S. Partially Averaged Navier-Stokes (PANS) Scale Resolving Simulations: From Fundamentals to Engineering Applications. In *Book: ERCOFTAC Bulletin 121: Progress in RANS-Based Scale-Resolving Flow Simulation Methods II*; ERCOFTAC: London, UK, 2019; pp. 25–32.
22. Stipic, M.; Basara, B.; Schmidt, S.; Adams, N. *Numerical Analysis of Combustion Process in the Dual Fuel Internal Combustion Engine*; SAE Technical Papers; SAE International: Detroit, MI, USA, 2023. [CrossRef]
23. Basara, B.; Pavlovic, Z.; Girimaji, S. A new approach for the calculation of the cut-off resolution parameter in bridging methods for turbulent flow simulation. *Int. J. Heat Fluid Flow* **2018**, *74*, 76–88. [CrossRef]
24. Girimaji, S.S.; Abdol-Hamid, K.S. Partially-averaged Navier Stokes Model for Turbulence: Implementation and Validation. In Proceedings of the 43rd AIAA Aerospace Sciences Meeting and Exhibit—Meeting Papers, Reno, Nevada, 10–13 January 2005; American Institute of Aeronautics and Astronautics Inc.: Reston, VA, USA, 2005; pp. 12887–12900. [CrossRef]
25. Girimaji, S.S. Partially-averaged navier-stokes model for turbulence: A reynolds-averaged navier-stokes to direct numerical simulation bridging method. *J. Appl. Mech.* **2006**, *73*, 413–421. [CrossRef]
26. Hanjalić, K.; Popovac, M.; Hadžiabdić, M. A robust near-wall elliptic-relaxation eddy-viscosity turbulence model for CFD. *Int. J. Heat Fluid Flow* **2004**, *25*, 1047–1051. [CrossRef]
27. Basara, B.; Krajnovi, S.; Girimaji, S.; Pavlovic, Z. Near-wall formulation of the partially averaged Navier-Stokes turbulence model. *AIAA J.* **2011**, *49*, 2627–2636. [CrossRef]

28. Li, K.; Rahnama, P.; Novella, R.; Somers, B. Combining flamelet-generated manifold and machine learning models in simulation of a non-premixed diffusion flame. *Energy AI* **2023**, *14*, 100266. [CrossRef]
29. Van Oijen, J.A.; Donini, A.; Bastiaans, R.J.M.; Boonkkamp, J.H.M.T.T.; de Goey, L.P.H. State-of-the-art in premixed combustion modeling using flamelet generated manifolds. *Prog. Energy Combust. Sci.* **2016**, *57*, 30–74. [CrossRef]
30. Kalbhor, A.; van Oijen, J. An assessment of the sectional soot model and FGM tabulated chemistry coupling in laminar flame simulations. *Combust. Flame* **2021**, *229*, 111381. [CrossRef]
31. AVL. *AVL FIRE General Gas Phase Reactions Manual*; AVL GmbH List: Graz, Austria, 2022.
32. Mehl, M.; Pitz, W.J.; Westbrook, C.K.; Curran, H.J. Kinetic modeling of gasoline surrogate components and mixtures under engine conditions. *Proc. Combust. Inst.* **2011**, *33*, 193–200. [CrossRef]
33. Lapointe, S.; Zhang, K.; McNenly, M.J. Reduced chemical model for low and high-temperature oxidation of fuel blends relevant to internal combustion engines. *Proc. Combust. Inst.* **2019**, *37*, 789–796. [CrossRef]
34. Chemical-Kinetic Mechanisms for Combustion Applications. San Diego Mechanism Web Page. Mechanical and Aerospace Engineering (Combustion Research), University of California at San Diego. Available online: web.eng.ucsd.edu/mae/groups/combustion/mechanism.html (accessed on 29 November 2023).
35. Pei, Y.; Mehl, M.; Liu, W.; Lu, T.; Pitz, W.J.; Som, S. A Multicomponent Blend as a Diesel Fuel Surrogate for Compression Ignition Engine Applications. *J. Eng. Gas Turbine Power* **2015**, *137*, 111502. [CrossRef]
36. Patankar, S.V.; Spalding, D.B. A calculation procedure for heat, mass and momentum transfer in three-dimensional parabolic flows. *Int. J. Heat Mass Transf.* **1972**, *15*, 1787–1806. [CrossRef]
37. Basara, B. Eddy Viscosity Transport Model Based on Elliptic Relaxation Approach. *AIAA J.* **2006**, *44*, 1686–1690. [CrossRef]
38. Gaballa, H.; Habchi, C.; de Hemptinne, J.-C. Modeling and LES of high-pressure liquid injection under evaporating and non-evaporating conditions by a real fluid model and surface density approach. *Int. J. Multiph. Flow* **2023**, *160*, 104372. [CrossRef]
39. Naber, J.; Reitz, R.D. Modeling Engine Spray/Wall Impingement. *SAE Techn. Pap. Ser.* **1988**, *22*, 880107. [CrossRef]
40. Alla, G.H.A.; Badr, O.A.; Soliman, H.A.; Rabbo, M.F.A. Technical note: Exhaust emissions from an indirect injection dual-fuel engine. *Proc. Inst. Mech. Eng. Part D J. Automob. Eng.* **2000**, *214*, 333–334. [CrossRef]
41. Kobayashi, H.; Ham, F.; Wu, X. Application of a local SGS model based on coherent structures to complex geometries. *Int. J. Heat Fluid Flow* **2008**, *29*, 640–653. [CrossRef]
42. Kobayashi, H. The subgrid-scale models based on coherent structures for rotating homogeneous turbulence and turbulent channel flow. *Phys. Fluids* **2005**, *17*, 045104. [CrossRef]
43. Jupudi, R.S.; Finney, C.E.; Primus, R.; Wijeyakulasuriya, S.; Klingbeil, A.E.; Tamma, B.; Stoyanov, M.K. *Application of High Performance Computing for Simulating Cycle-to-Cycle Variation in Dual-Fuel Combustion Engines*; SAE Technical Papers; SAE International: Detroit, MI, USA, 2016. [CrossRef]
44. Pasunurthi, S.; Jupudi, R.; Wijeyakulasuriya, S.; Gubba, S.R.; Im, H.; Ali, M.J.M.; Primus, R.; Klingbeil, A.; Finney, C. *Cycle to Cycle Variation Study in a Dual Fuel Operated Engine*; SAE Technical Papers; SAE International: Detroit, MI, USA, 2017. [CrossRef]
45. Gubba, S.R.; Jupudi, R.S.; Kodavasal, J.; Som, S.; Primus, R.J.; Klingbeil, A.E.; Finney, C.; Wijeyakulasuriya, S.D. Development of Predictive Capability of Cycle-to-Cycle Variation in Dual-Fuel Engines using Supercomputing-based Computational Fluid Dynamics. In Proceedings of the FISTA World Automotive Congress 2018, Chennai, India, 2–5 October 2018.